Title: Neurodevelopmental disorder risk gene *DYRK1A* is required for ciliogenesis and brain size in *Xenopus* embryos

Authors: Helen Rankin Willsey[1,2‡], Yuxiao Xu[1,2‡], Amanda Everitt[3], Jeanselle Dea[1], Cameron R. T. Exner[1], A. Jeremy Willsey[3*], Matthew W. State[1*], Richard M. Harland[2*]

Affiliations:

[1]Department of Psychiatry, Weill Institute for Neurosciences, Quantitative Biosciences Institute, University of California San Francisco, San Francisco, CA

[2]Department of Molecular and Cell Biology, University of California, Berkeley, Berkeley, CA

[3]Department of Psychiatry, Institute for Neurodegenerative Diseases, Weill Institute for Neurosciences, Quantitative Biosciences Institute, University of California San Francisco, San Francisco, CA

*Correspondence: harland@berkeley.edu, matthew.state@ucsf.edu, jeremy.willsey@ucsf.edu

‡These authors contributed equally

Key words: DYRK1A, ciliogenesis, autism, Down Syndrome, microtubules, spindle

Summary Statement: Autism and Down Syndrome risk gene DYRK1A localizes to ciliary components and mitotic spindles, and is required for ciliogenesis and cell cycle control during embryonic *Xenopus* development.

Abstract: *DYRK1A* (dual specificity tyrosine-(Y)-phosphorylation-regulated kinase 1 A) is a high confidence autism risk gene that encodes a conserved kinase. In addition to autism, patients with putative loss of function variants in *DYRK1A* exhibit microcephaly, intellectual disability, developmental delay, and/or congenital anomalies of the kidney and urinary tract. *DYRK1A* is also located within the critical region for Down syndrome; therefore, understanding the role of *DYRK1A* in brain development is crucial for understanding the pathobiology of multiple developmental disorders. To characterize the function of this gene, we used the diploid frog, *Xenopus tropicalis*. We discover that Dyrk1a is expressed in ciliated tissues, localizes to ciliary axonemes and basal bodies, and is required for ciliogenesis. We also demonstrate that Dyrk1a localizes to mitotic spindles and that its inhibition leads to decreased forebrain size, abnormal cell cycle progression, and cell death during brain development. These findings provide hypotheses about potential mechanisms of pathobiology and underscore the utility of *X. tropicalis* as a model system for understanding neurodevelopmental disorders.

Introduction:

DYRK1A (Dual specificity tyrosine-(Y)-phosphorylation-regulated kinase 1 A) encodes a highly conserved serine-threonine protein kinase expressed during human embryonic brain development (van Bon et al. 2016). Large-scale human genetics efforts have rigorously associated *DYRK1A* mutations with numerous developmental disorders (van Bon et al. 2015; Feki and Hibaoui 2018). Specifically, *DYRK1A* is a high-confidence risk gene for autism spectrum disorders (ASD) (Satterstrom et al. 2020; Iossifov et al. 2012). More recently, *DYRK1A* haploinsufficiency has been proposed to cause a distinct syndrome, characterized by ASD along with microcephaly, intellectual disability, developmental delay, and/or congenital anomalies of the kidney and urinary tract (van Bon et al. 2016; Earl et al. 2017; Ji et al. 2015; Blackburn et al. 2019). *DYRK1A* is located within the Down syndrome critical region on chromosome 21, and increased dosage of *DYRK1A* has been implicated in Down syndrome pathobiology (Arron et al. 2006). Accordingly, DYRK1A kinase inhibitors are currently being explored for therapeutic potential (Neumann et al. 2018; Feki and Hibaoui 2018; Duchon and Herault 2016).

The function of *DYRK1A* in brain development has been studied in a wide range of model systems. The microcephaly observed in human patients with *DYRK1A* haploinsufficiency is recapitulated in both *Drosophila* and mouse heterozygous mutant animals (Fotaki et al. 2002; Tejedor et al. 1995). Mice with *DYRK1A* heterozygous mutations also display motor deficits, developmental delay, and altered behavior (Fotaki et al. 2002; Dierssen and de Lagrán 2006; Arqué et al. 2009). At the cellular level, there is evidence that *DYRK1A* is required for cell cycle control, differentiation, and dendritic spine development (Shaikh et al. 2016; Ori-McKenney et al. 2016; Dang et al. 2018). Molecularly, DYRK1A has been shown to phosphorylate a wide range of target proteins including mRNA splicing factors (de Graaf et al. 2006; Shi et al. 2008), transcription factors (Fernandez-Martinez et al. 2009; Ehe et al. 2017; Mao et al. 2002), cyclins (Smith and Calegari 2015; Soppa et al. 2014; Najas et al. 2015; Chen et al. 2013), and β-Tubulin (Ori-McKenney et al. 2016). However, it is unknown which of these functions are central to the role of DYRK1A in brain development and which underlie pathobiology of related conditions.

Here we characterize the expression, localization, and function of Dyrk1a in *Xenopus tropicalis* embryos to better understand its role in development. We uncover a novel localization of Dyrk1a to ciliary components and a corresponding novel requirement for Dyrk1a in ciliogenesis. Furthermore, we describe a novel localization of Dyrk1a to mitotic spindles and demonstrate that inhibition alters cell cycle progression and cell survival in the developing brain.

These observations suggest underlying deficits in microtubule dynamics, for which Dyrk1a has a known role (Ori-McKenney et al. 2016). Finally, we observe a marked reduction in forebrain size following *dyrk1a* loss of function, a phenotype consistent with human *DYRK1A* haploinsufficiency and deficits in cell cycle progression.

Results and Discussion:

Expression and localization of Dyrk1a during* X. tropicalis *development

By whole-mount RNA *in situ* hybridization, we detected *dyrk1a* mRNA throughout *X. tropicalis* embryonic development, spanning gastrulation (Fig. 1A), neurulation (Fig. 1B), and organogenesis (Fig. 1C-F). Expression is strong in neural and ciliated tissues, including the embryonic epidermis (Fig. 1B), the developing brain and eye, the otic vesicle, and the pronephros (Fig 1C-E, (Blackburn et al. 2019)). It is also expressed in the pharyngeal arches and developing heart (Fig. 1C-D). During neurogenesis, it is highly expressed in the proliferative cells lining the brain ventricles (Fig. 1E). Later, it is expressed throughout the tadpole brain, in the telencephalon (tel), diencephalon (di), mesencephalon (mes), and rhombencephalon (rhomb) (Fig. 1F).

By antibody staining of tailbud stages, we detected endogenous *Xenopus* Dyrk1a protein in puncta along ciliary axonemes, labeled by acetylated α-Tubulin (Fig. 1G). This staining is lost following *dyrk1a* depletion by morpholino oligonucleotides (MO) or by CRISPR/Cas9-mediated mutagenesis (Fig. S1). In tadpole stages, Dyrk1a antibody staining shows specific labeling throughout the brain (Fig. 1H), and especially in ciliated cells such as the olfactory epithelium (olf, Fig. 1I) and the roof of the fourth ventricle in the rhombencephalon (rhomb, Fig. 1J). We confirmed ciliary localization with a GFP-tagged human DYRK1A (hDYRK1A-GFP) expressed in the *Xenopus* embryonic epidermis. Human DYRK1A also localized in puncta along ciliary axonemes (Fig. 1K) and at ciliary basal bodies labeled with Centrin-CFP (Fig. 1L). These results demonstrate that Dyrk1a is expressed in neural and ciliated tissues during embryonic development and localizes to ciliary axonemes.

dyrk1a *is required for ciliogenesis and telencephalon size*

To investigate the function of Dyrk1a, we disrupted endogenous expression with either MO knock-down or CRISPR/Cas9 mutagenesis. This *dyrk1a* translation-blocking MO has previously been validated in *Xenopus* kidney development (Blackburn et al. 2019). We confirmed that the single guide RNA (sgRNA) targeting *dyrk1a* was efficient by Sanger sequencing and sequence deconvolution (mean efficiency 71%, standard deviation 18%; Fig.

S2). In both cases, these loss of function strategies abolished Dyrk1a antibody staining in the ciliated epidermis in tailbud stages (Fig. S1). Therefore, we assayed whether ciliogenesis was disrupted following loss of *dyrk1a* by either strategy. In both cases, we observed that depletion of Dyrk1a during embryonic development leads to ciliogenesis defects (Fig. 2A-D, Fig. S3).

Because human patients with *DYRK1A* haploinsufficiency have microcephaly, we next assayed the gross brain anatomy of *dyrk1a* loss of function animals at the tadpole stages by labeling neurons with β-Tubulin antibody staining. We injected MO or CRISPR/Cas9 components into 1 cell at the 2-cell stage, generating unilateral loss of *dyrk1a* function, where the uninjected half serves as a contralateral control (H. R. Willsey et al. 2018; DeLay et al. 2018; Lasser et al. 2019). Loss of *dyrk1a* function by either method led to a reduction in telencephalon size without a dramatic alteration in gross regional anatomy (Fig. 2E-F, I, both $p < 0.05$ by Mann-Whitney rank sum test compared to negative control pigmentation gene *slc45a2*). In both this assay and in the ciliogenesis assay, the MO injection produced a stronger effect than the CRISPR injection, potentially because of the presence of maternal *dyrk1a* mRNA (Owens et al. 2016) that will only be targeted by the MO. We were able to rescue the reduction in telencephalon size following CRISPR injection by co-injection of *hDYRK1A-GFP* (Fig. 2H-I), suggesting conservation of function. Finally, we validated this loss of function phenotype by inhibition of Dyrk1a kinase activity using a validated pharmacological inhibitor Harmine (Göckler et al. 2009) (Fig. 2G, $p < 0.05$). Together these results demonstrate that *dyrk1a* is required for ciliogenesis and telencephalon size control during *Xenopus* embryonic development.

RNA sequencing implicates cell cycle control in* dyrk1a *brain phenotype

To understand how *dyrk1a* loss of function leads to a smaller telencephalon, we sequenced RNA from dissected brains from control and *dyrk1a* CRISPR-injected animals at stage 46 (Fig. 3). After sequencing, we first confirmed that CRISPR/Cas9 resulted in mRNA disruption by analyzing sequence reads surrounding the protospacer adjacent motif (PAM) site within the target exon of *dyrk1a*. We observed a depletion of sequencing depth in all three injected replicates but not in control replicates (Fig. 3A), suggesting efficient targeting. Next, we identified 294 differentially expressed genes (Fig. 3B, Table S1), of which 172 were upregulated (orange points) and 122 were downregulated (blue points). Gene ontology enrichment analysis of the differentially expressed genes demonstrated strong enrichment in biological processes related to cell cycle control, DNA replication, and microtubules (Fig. 3C, Table S2). Strikingly, canonical cell cycle genes such as *cyclin dependent kinase 1*, *aurora kinase B*, and *cyclins B1, B2,* and *A2* are all increased greater than two-fold (Fig. 3D, Table S1). Therefore, we

hypothesized that the small telencephalon phenotype may be due to disruption of cell cycle progression.

It has previously been shown that loss of *dyrk1a* speeds the transition from Gap 1 (G1) phase to Synthesis (S) phase due to its role in regulating Cyclin D degradation (Chen et al. 2013; Najas et al. 2015; Soppa et al. 2014). However, our observations also suggest a novel role for Dyrk1a in regulating mitotic (M) phase. Specifically, we observed upregulation of *cyclin B1* and *B2,* two genes known to reach maximum mRNA expression during the M phase of the cell cycle (Ito 2000). We also observed enrichment of microtubule-related processes, including gene ontology terms related to the mitotic spindle. These data, combined with the fact that Dyrk1a localizes to ciliary axonemes and is required for ciliogenesis, a process that requires dynamic microtubule remodeling, led us to hypothesize that Dyrk1a may impact M phase via a role in mitotic spindle dynamics. This idea is consistent with a previously described function for Dyrk1a in regulating microtubule dynamics in developing dendrites (Ori-McKenney et al. 2016). Therefore, we stained blastula stage embryos, which are highly mitotic, for endogenous Dyrk1a. Remarkably, we observed a clear and novel localization near mitotic spindles marked by α-Tubulin (Fig. 4A-B). Together, these findings suggest that *dyrk1a* is important for cell cycle progression, possibly by modulating microtubule dynamics and/or the mitotic spindle, and that loss may cause stalling during the M phase of the cell cycle.

Dyrk1a is required for cell cycle progression and survival

Next we used the validated Dyrk1a kinase inhibitor Harmine to determine whether cell cycle progression is indeed affected following loss of Dyrk1a function. This perturbation also results in the small telencephalon phenotype seen with the genetic inhibitors (Fig. 2G,I), but has the advantage of enhanced temporal control, and thus, the ability to bypass early embryonic roles of Dyrk1a. Consistent with the RNA-Seq data and the known role of Dyrk1a in regulating Cyclin D, we observed an increase in the number of cells expressing the S phase marker PCNA (proliferating cell nuclear antigen) in the developing brain (Fig. 4C-E, $p < 0.0001$ by Mann-Whitney rank sum test) as well as a relative increase in these cells compared to the rest of the telencephalon (Fig. 4F, $p = 0.0045$). Dyrk1a inhibition also caused an increase in cells labeled by phospho-histone H3 (pHH3), a marker for M phase (Fig. 4G-I, $p < 0.0001$, Fig. S4C-D), suggesting that more cells are in M phase. We also observed an increase in cleaved caspase 3 (CCP3) staining following Dyrk1a inhibition (Fig. 4J-L, $p < 0.0001$), or following MO or CRISPR injection (Fig. S4A-B). These results generate hypotheses about the apparent paradox between a smaller brain (Fig. 2) and an increase in markers of proliferation (Fig. 3). It is possible that

stalling in M phase, perhaps through disruption of the mitotic spindle, could increase the number of apparently proliferative cells, yet lead to a decrease in forebrain size, especially if stalling induces apoptosis. Alternatively, rapid progression into S phase could underlie the increase in M phase cells and cell death. Regardless, these data point to a clear role for Dyrk1a in cell cycle progression and survival during *Xenopus* neurogenesis.

In summary, this work reveals a novel role for Dyrk1a in embryonic ciliogenesis and a putative novel role at mitotic spindles during mitosis. Both processes require dynamic microtubule remodeling, and Dyrk1a has been shown to directly regulate microtubule dynamics during dendrite development (Ori-McKenney et al. 2016). Therefore, we hypothesize that the ciliogenesis and cell cycle phenotypes observed following loss of Dyrk1a both arise from an underlying deficit in microtubule dynamics. Future work should directly explore the role of Dyrk1a in mitotic spindle function. It should also determine if cells are stalled in M phase rather than transitioning quickly from G1 to S thereby resulting in an increase of M phase cells. It is also important to understand the mechanism underlying cell death, as well as its relative contribution to the observed small forebrain phenotype, compared to cell cycle progression defects. Furthermore, the observed defects in ciliogenesis suggest that potential disruptions of basal bodies and primary cilia should be investigated, as well as concomitant changes in patterning.

Overall, these findings provide insight into the pathobiology underlying *DYRK1A* haploinsufficiency. The identification of conserved phenotypes (microcephaly) between human *DYRK1A* haploinsufficiency and *Xenopus dyrk1a* loss of function reinforces the utility of this model organism for studying developmental disorder risk genes being identified in large scale genetics efforts (A. J. Willsey et al. 2018; Satterstrom et al. 2020) and informs current studies testing DYRK1A kinase inhibitors as potential therapeutics for Down Syndrome and Alzheimer's Disease (Branca et al. 2017; Stotani, Giordanetto, and Medda 2016; Feki and Hibaoui 2018; Duchon and Herault 2016; Neumann et al. 2018), as it predicts side effects in ciliated and proliferative tissues. This work also suggests that the congenital kidney and urogenital tract abnormalities in patients with *DYRK1A* haploinsufficiency may be due to underlying ciliogenesis defects and that these patients should be carefully evaluated for other cilia-related disorders, such as congenital heart disease, hydrocephalus, and retinal degeneration.

Materials and Methods*:*

***Xenopus* husbandry:** *Xenopus tropicalis* adult animals were maintained and cared for according to established IACUC protocols. Animals were wildtype and both sexes were used. Animals were ovulated with human chorionic gonadotropin (Sigma) according to (Sive, Grainger, and Harland 2000), and both *in vitro* fertilizations and natural matings were utilized. Embryos were staged according to (Nieuwkoop and Faber 1958).

Whole mount RNA *in situ* hybridization: *X. tropicalis dyrk1a* cDNA IMAGE clone 7687837 (Morin et al. 2006) and digoxygenin-11-UTP were used to synthesize antisense probe according to standard protocol using SalI restriction enzyme and T7 polymerase (Sive, Grainger, and Harland 2007). Embryos were fixed and stained according to standard protocol (Harland 1991), with the omission of the proteinase K step when assaying expression in the multiciliated cells on the epidermis.

Plasmids & cloning: Full-length human *DYRK1A* cDNA (transcript NM_001396) was obtained from the Harvard Plasmid repository (HsCD00082867) and cloned into pDONR221. LR cloning reactions added an N-terminal GFP using destination vector *pCS-EGFP*, a kind gift from John Wallingford (Tu et al. 2018). Sanger sequencing verified the sequences (ElimBio). *Centrin-CFP* was a kind gift from Peter Walentek (Walentek et al. 2016; Antoniades, Stylianou, and Skourides 2014; Park et al. 2008).

Embryonic injections: Embryos were injected with 2 nl per blastomere into 1 cell at the 2-cell stage using a Narishige micromanipulator and a Parker Picospritzer III. Plasmid (*hDYRK1A-GFP*) was injected at 40 pg per embryo and mRNA (*Centrin-CFP*) was injected at 500 pg per embryo. Morpholino was injected at 2 ng per embryo; sgRNA was injected at 800 pg per embryo; and Cas9-NLS protein (MacroLabs, UC Berkeley, (Lingeman, Jeans, and Corn 2017)) was injected at 1.5 ng per embryo. Fluorescent dextrans were co-injected to label the injected side of the embryo and animals were sorted left from right-injected at neurula stages.

Fluorescence staining: Immunostaining was carried out according to (H. R. Willsey et al. 2018), with the omission of the bleaching step whenever phalloidin was included. Phalloidin was added during the secondary antibody incubation to visualize actin (1:50, Life Technologies A12380 or A22287). Mounting media with DAPI was used to visualize DNA (Vectashield, Fisher NC9524612). The following primary antibodies were used: DYRK1A (1:100, Abcam ab69811), acetylated α-Tubulin (1:700, Sigma T6793), β-Tubulin (1:100, DSHB clone E7), PCNA (1:50,

Life Technologies, clone PC10), polyglutamylated Tubulin (1:100, AdipoGen GT335), phospho-histone H3 (1:100, Ser10, Sigma #06-570), and cleaved caspase 3 (1:100, Asp175, Cell Signaling #9661). Secondary fluorescence-conjugated antibodies were used at 1:250 (Life Technologies).

***dyrk1a* loss of function:** Published and validated translation-blocking *dyrk1a* morpholino (5' TGCATCGTCCTCTTTCAAGTCTCAT 3') (Blackburn et al. 2019) was injected at 2 ng per embryo. sgRNA against *X. tropicalis dyrk1a* was designed using CRISPRscan (Moreno-Mateos et al. 2015) (target sequence: 5'-CGTTTAGGTTCTGCTGACGGCGG-3', oligo sequence: 5'-taatacgactcactataGGTTTAGGTTCTGCTGACGGgttttagagctagaa-3') and was synthesized *in vitro* (Engen) and purified (Zymo). Purified Cas9-NLS protein was acquired from MacroLab (UC Berkeley) (Lingeman, Jeans, and Corn 2017). For genotyping, genomic DNA was isolated and the region around the protospacer adjacent motif (PAM) site was amplified by PCR using primers (F: 5'-GGAGAAATCCCTGACAATTGTATTAATTATAGCATTG-3' and R: 5'-GTTCTTGACCGGTACTGACAAAATGAG-3'), and Sanger sequenced. Mutational efficiency was estimated by sequence deconvolution by tracking of INDELs (TIDE) (Brinkman et al. 2014; DeLay et al. 2018).

Drug Treatment: DYRK1A inhibitor harmine (Sigma Aldrich, 286044) (Göckler et al. 2009; Bain et al. 2007) was reconstituted in dimethylsulfoxide (DMSO) as a 1 mM stock solution. Animals were treated with 1.25 µM of harmine in 1/9 modified ringers or an equal volume of DMSO in 1/9 modified ringers at stage 30, unless otherwise indicated. The embryos were raised until fixation at stage 46 for immunofluorescence staining. Culture liquid was not refreshed during treatment for either condition. Dead animals were removed as soon as they were observed.

Microscopy: RNA *in situ* hybridization embryos were visualized on a Zeiss AxioZoom.V16 with a 1X objective and a Zeiss 105 color camera with extended depth of focus. Localization and cilia images were acquired on a Leica SP8 laser scanning confocal with a 63X objective. Tadpole nervous system images were acquired by Zeiss AxioZoom.V16 with a 1X objective with a Zeiss 506 monochrome camera and apotome. Whole-mount images are maximum intensity projections of optical sections. We have previously shown that our antibody staining protocol penetrates the brain and that this imaging strategy is sufficient to detect the same gross size changes as physical transverse sections (H. R. Willsey et al. 2018).

Image analyses & statistical analyses: Images were processed in FIJI (NIH) and compiled in Illustrator (Adobe). Differences in area were measured in FIJI using the free-hand selection function followed by the measure function. Cells with positive antibody staining were marked and counted manually in FIJI. Differences in mean area or cell number were tested for statistical significance by non-parametric Mann-Whitney rank sum test (GraphPad Prism 8).

RNA extraction, library preparation, & sequencing: Individual brains from control and bilaterally injected *dyrk1a* CRISPR tadpoles were dissected at stage 46 and immediately put in 200 µl of cold Trizol (Thermo Fisher), pipetted with a 30 gauge needle to dissociate, and frozen at -80^{o}C. Carcasses were genotyped to determine mutational efficiency, and the nine most mutagenized brains were selected and pooled into 3 independent replicates (3 brains per replicate). 9 uninjected brains were pooled into 3 independent replicates (3 brains per replicate). RNA extraction, polyA selection, and low-input library preparation (500 bp size selection) were performed by the Functional Genomics Laboratory (UC Berkeley). Samples were processed together, barcoded, and spread across a sequencing lane to reduce batch effects. Unstranded, 150 paired end sequencing was performed on an Illumina HiSeq 4000 by the Genomics Sequencing Laboratory (UC Berkeley).

Transcriptome analysis: RNA-Seq reads were aligned to the XenBase *X. tropicalis* v9.1 reference genome using STAR v2.7.3 (Dobin et al. 2013) in gene annotation mode with default parameters. Read counts were converted into counts per million (cpm) and genes with more than 1 cpm in at least 3 samples were retained for differential gene expression (DEX) analysis. Filtered genes were tested for differential expression using DESeq2 v1.24.0 (Love, Huber, and Anders 2014) with shrinkage estimator apeglm (Zhu, Ibrahim, and Love 2019). p-values were corrected for multiple testing using the Benjamini and Hochberg FDR correction. Significantly DEX genes are genes that pass a 0.05 significant threshold. Gene Ontology (GO) enrichment analysis of all annotated DEX genes (N=221) was performed using the online classification tool PANTHER (Mi et al. 2010) against the available *Xenopus* database using all expressed genes as a background (N=15079).

Because DYRK1A has been shown to phosphorylate splicing factors (de Graaf et al. 2006; Shi et al. 2008), we also analyzed the data to identify differentially expressed exons. DEXseq (Anders, Reyes, and Huber 2012) with default parameters was used to quantify exon-level counts and subsequently identify differential exon usage between wildtype and *dyrk1a* knockdown samples. Genes with total exon-level counts below 5 were removed before

differential exon usage (DEU) analysis. p-values per exon were corrected for multiple testing using the Benjamini and Hochberg FDR correction. There were 97 identified DEU sites within 82 genes which passed a 0.05 significance threshold (Table S3).

Acknowledgements: We thank Mustafa Khokha and Michael Slocum for wildtype frogs and husbandry advice; Nolan Wong, Kelly Jensen, Gary Moulder, Louie Ramos, and Shaun Coughlin for support at the UCSF *Xenopus* facility; James Evans for support at the UC Berkeley *Xenopus* facility; Edivinia Pangilinan for expert technical help; Xenbase (RRID:SCR_003280) for essential, daily reference; the National *Xenopus* Resource (RRID:SCR_013731) for wildtype *X. tropicalis* and technical advice with husbandry and genotyping; CSHL *Xenopus* Course (2015-2019); John Wallingford for pCS-EGFP Gateway vector; A.J.W. for endless support and L.S.W. for inspiration. We acknowledge support from the Overlook International Foundation and the Weill Institute for Neurosciences. This work used the Vincent J. Coates Genomics Sequencing Laboratory at UC Berkeley, supported by National Institutes of Health S10 OD018174 Instrumentation Grant. This work is a component of the NIMH Convergent Neuroscience Initiative and the Psychiatric Cell Mapping Initiative (pcmi.ucsf.edu) and was supported by National Institutes of Health grant 1U01MH115747-01A1 to A.J.W. and M.W.S..

Competing Interests: A.J.W. is a consultant for Daiichi Sankyo and M.W.S. is a consultant for BlackThorn Therapeutics. No competing interests declared by any other authors.

Funding: This work was supported by National Institutes of Mental Health grant 1R21MH112158-01 and National Institute of General Medical Sciences grant R35GM127069 to R.M.H. This work is a component of the National Institutes of Mental Health Convergent Neuroscience Initiative and was supported by National Institutes of Mental Health grant 1U01MH115747-01A1 to A.J.W. and M.W.S..

Data Availability: The data discussed in this publication have been deposited in NCBI's Gene Expression Omnibus (Edgar et al., 2002) and are accessible through GEO Series accession number GSE149538 (https://www.ncbi.nlm.nih.gov/geo/query/acc.cgi?acc=GSE149538).

References:

Anders, Simon, Alejandro Reyes, and Wolfgang Huber. 2012. “Detecting Differential Usage of Exons from RNA-Seq Data.” *Genome Research* 22 (10): 2008–17.

Antoniades, Ioanna, Panayiota Stylianou, and Paris A. Skourides. 2014. “Making the Connection: Ciliary Adhesion Complexes Anchor Basal Bodies to the Actin Cytoskeleton.” *Developmental Cell* 28 (1): 70–80.

Arqué, Glòria, María Martínez de Lagrán, Maria L. Arbonés, and Mara Dierssen. 2009. “Age-Associated Motor and Visuo-Spatial Learning Phenotype in Dyrk1A Heterozygous Mutant Mice.” *Neurobiology of Disease* 36 (2): 312–19.

Arron, Joseph R., Monte M. Winslow, Alberto Polleri, Ching-Pin Chang, Hai Wu, Xin Gao, Joel R. Neilson, et al. 2006. “NFAT Dysregulation by Increased Dosage of DSCR1 and DYRK1A on Chromosome 21.” *Nature* 441 (7093): 595–600.

Bain, Jenny, Lorna Plater, Matt Elliott, Natalia Shpiro, C. James Hastie, Hilary McLauchlan, Iva Klevernic, J. Simon C. Arthur, Dario R. Alessi, and Philip Cohen. 2007. “The Selectivity of Protein Kinase Inhibitors: A Further Update.” *Biochemical Journal* 408 (3): 297–315.

Blackburn, Alexandria T. M., Nasim Bekheirnia, Vanessa C. Uma, Mark E. Corkins, Yuxiao Xu, Jill A. Rosenfeld, Matthew N. Bainbridge, et al. 2019. “DYRK1A-Related Intellectual Disability: A Syndrome Associated with Congenital Anomalies of the Kidney and Urinary Tract.” *Genetics in Medicine: Official Journal of the American College of Medical Genetics* 21 (12): 2755–64.

Bon, Bregje W. M. van, Bradley P. Coe, Bert B. A. de Vries, and Evan E. Eichler. 2015. “DYRK1A-Related Intellectual Disability Syndrome.” In *GeneReviews*, edited by Margaret P. Adam, Holly H. Ardinger, Roberta A. Pagon, Stephanie E. Wallace, Lora J. H. Bean, Karen Stephens, and Anne Amemiya. Seattle (WA): University of Washington, Seattle.

Bon, B. W. M. van, B. P. Coe, R. Bernier, C. Green, J. Gerdts, K. Witherspoon, T. Kleefstra, et al. 2016. “Disruptive de Novo Mutations of DYRK1A Lead to a Syndromic Form of Autism and ID.” *Molecular Psychiatry* 21 (1): 126–32.

Branca, Caterina, Darren M. Shaw, Ramona Belfiore, Vijay Gokhale, Arthur Y. Shaw, Christopher Foley, Breland Smith, et al. 2017. “Dyrk1 Inhibition Improves Alzheimer’s Disease-like Pathology.” *Aging Cell* 16 (5): 1146–54.

Brinkman, Eva K., Tao Chen, Mario Amendola, and Bas van Steensel. 2014. “Easy Quantitative Assessment of Genome Editing by Sequence Trace Decomposition.” *Nucleic Acids Research* 42 (22): e168.

Chen, Jia-Yun, Jia-Ren Lin, Feng-Chiao Tsai, and Tobias Meyer. 2013. “Dosage of Dyrk1a Shifts Cells within a p21-Cyclin D1 Signaling Map to Control the Decision to Enter the Cell Cycle.” *Molecular Cell* 52 (1): 87–100.

Dang, T., W. Y. Duan, B. Yu, D. L. Tong, C. Cheng, Y. F. Zhang, W. Wu, et al. 2018. “Autism-Associated Dyrk1a Truncation Mutants Impair Neuronal Dendritic and Spine Growth and Interfere with Postnatal Cortical Development.” *Molecular Psychiatry* 23 (3): 747–58.

DeLay, Bridget D., Mark E. Corkins, Hannah L. Hanania, Matthew Salanga, Jian Min Deng, Norihiro Sudou, Masanori Taira, Marko E. Horb, and Rachel K. Miller. 2018. “Tissue-Specific Gene Inactivation in Xenopus Laevis: Knockout of lhx1 in the Kidney with CRISPR/Cas9.” *Genetics*. https://doi.org/10.1534/genetics.117.300468.

Dierssen, M., and M. Martínez de Lagrán. 2006. “DYRK1A (dual-Specificity Tyrosine-Phosphorylated and -Regulated Kinase 1A): A Gene with Dosage Effect during Development and Neurogenesis.” *TheScientificWorldJournal* 6 (June): 1911–22.

Dobin, Alexander, Carrie A. Davis, Felix Schlesinger, Jorg Drenkow, Chris Zaleski, Sonali Jha, Philippe Batut, Mark Chaisson, and Thomas R. Gingeras. 2013. “STAR: Ultrafast Universal RNA-Seq Aligner.” *Bioinformatics* 29 (1): 15–21.

Duchon, Arnaud, and Yann Herault. 2016. “DYRK1A, a Dosage-Sensitive Gene Involved in Neurodevelopmental Disorders, Is a Target for Drug Development in Down Syndrome.” *Frontiers in Behavioral Neuroscience* 10 (June): 104.
Earl, Rachel K., Tychele N. Turner, Heather C. Mefford, Caitlin M. Hudac, Jennifer Gerdts, Evan E. Eichler, and Raphael A. Bernier. 2017. “Clinical Phenotype of ASD-Associated DYRK1A Haploinsufficiency.” *Molecular Autism*. https://doi.org/10.1186/s13229-017-0173-5.
Edgar, Ron, Michael Domrachev, and Alex E. Lash. 2002. “Gene Expression Omnibus: NCBI Gene Expression and Hybridization Array Data Repository.” Nucleic Acids Research 30 (1): 207–10.
Ehe, Ben K., David R. Lamson, Michael Tarpley, Rob U. Onyenwoke, Lee M. Graves, and Kevin P. Williams. 2017. “Identification of a DYRK1A-Mediated Phosphorylation Site within the Nuclear Localization Sequence of the Hedgehog Transcription Factor GLI1.” *Biochemical and Biophysical Research Communications* 491 (3): 767–72.
Feki, Anis, and Youssef Hibaoui. 2018. “DYRK1A Protein, A Promising Therapeutic Target to Improve Cognitive Deficits in Down Syndrome.” *Brain Sciences* 8 (10). https://doi.org/10.3390/brainsci8100187.
Fernandez-Martinez, Javier, Eva M. Vela, Mireille Tora-Ponsioen, Oscar H. Ocaña, M. Angela Nieto, and Juan Galceran. 2009. “Attenuation of Notch Signalling by the Down-Syndrome-Associated Kinase DYRK1A.” *Journal of Cell Science* 122 (Pt 10): 1574–83.
Firth, Helen V., Shola M. Richards, A. Paul Bevan, Stephen Clayton, Manuel Corpas, Diana Rajan, Steven Van Vooren, Yves Moreau, Roger M. Pettett, and Nigel P. Carter. 2009. “DECIPHER: Database of Chromosomal Imbalance and Phenotype in Humans Using Ensembl Resources.” *American Journal of Human Genetics* 84 (4): 524–33.
Fotaki, Vassiliki, Mara Dierssen, Soledad Alcántara, Salvador Martínez, Eulàlia Martí, Caty Casas, Joana Visa, Eduardo Soriano, Xavier Estivill, and Maria L. Arbonés. 2002. “Dyrk1A Haploinsufficiency Affects Viability and Causes Developmental Delay and Abnormal Brain Morphology in Mice.” *Molecular and Cellular Biology* 22 (18): 6636–47.
Göckler, Nora, Guillermo Jofre, Chrisovalantis Papadopoulos, Ulf Soppa, Francisco J. Tejedor, and Walter Becker. 2009. “Harmine Specifically Inhibits Protein Kinase DYRK1A and Interferes with Neurite Formation.” *The FEBS Journal* 276 (21): 6324–37.
Graaf, Katrin de, Hanna Czajkowska, Sabine Rottmann, Len C. Packman, Richard Lilischkis, Bernhard Lüscher, and Walter Becker. 2006. “The Protein Kinase DYRK1A Phosphorylates the Splicing Factor SF3b1/SAP155 at Thr434, a Novel in Vivo Phosphorylation Site.” *BMC Biochemistry* 7 (March): 7.
Harland, Richard M. 1991. “Appendix G: In Situ Hybridization: An Improved Whole-Mount Method for Xenopus Embryos.” *Methods in Cell Biology*. https://doi.org/10.1016/s0091-679x(08)60307-6.
Iossifov, Ivan, Michael Ronemus, Dan Levy, Zihua Wang, Inessa Hakker, Julie Rosenbaum, Boris Yamrom, et al. 2012. “De Novo Gene Disruptions in Children on the Autistic Spectrum.” *Neuron* 74 (2): 285–99.
Ito, M. 2000. “Factors Controlling Cyclin B Expression.” *Plant Molecular Biology* 43 (5-6): 677–90.
Ji, Jianling, Hane Lee, Bob Argiropoulos, Naghmeh Dorrani, John Mann, Julian A. Martinez-Agosto, Natalia Gomez-Ospina, et al. 2015. “DYRK1A Haploinsufficiency Causes a New Recognizable Syndrome with Microcephaly, Intellectual Disability, Speech Impairment, and Distinct Facies.” *European Journal of Human Genetics: EJHG* 23 (11): 1473–81.
Lasser, Micaela, Benjamin Pratt, Connor Monahan, Seung Woo Kim, and Laura Anne Lowery. 2019. “The Many Faces of Xenopus: Xenopus Laevis as a Model System to Study Wolf–Hirschhorn Syndrome.” *Frontiers in Physiology*. https://doi.org/10.3389/fphys.2019.00817.

Lingeman, Emily, Chris Jeans, and Jacob E. Corn. 2017. “Production of Purified CasRNPs for Efficacious Genome Editing.” Current Protocols in Molecular Biology / Edited by Frederick M. Ausubel ... [et Al.] 120 (October): 31.10.1–31.10.19.
Love, Michael I., Wolfgang Huber, and Simon Anders. 2014. “Moderated Estimation of Fold Change and Dispersion for RNA-Seq Data with DESeq2.” Genome Biology 15 (12): 550.
Mao, Junhao, Peter Maye, Priit Kogerman, Francisco J. Tejedor, Rune Toftgard, Wei Xie, Guanqing Wu, and Dianqing Wu. 2002. “Regulation of Gli1 Transcriptional Activity in the Nucleus by Dyrk1.” *The Journal of Biological Chemistry* 277 (38): 35156–61.
Mi, Huaiyu, Qing Dong, Anushya Muruganujan, Pascale Gaudet, Suzanna Lewis, and Paul D. Thomas. 2010. “PANTHER Version 7: Improved Phylogenetic Trees, Orthologs and Collaboration with the Gene Ontology Consortium.” *Nucleic Acids Research* 38 (Database issue): D204–10.
Moreno-Mateos, Miguel A., Charles E. Vejnar, Jean-Denis Beaudoin, Juan P. Fernandez, Emily K. Mis, Mustafa K. Khokha, and Antonio J. Giraldez. 2015. “CRISPRscan: Designing Highly Efficient sgRNAs for CRISPR-Cas9 Targeting in Vivo.” *Nature Methods* 12 (10): 982–88.
Morin, Ryan D., Elbert Chang, Anca Petrescu, Nancy Liao, Malachi Griffith, William Chow, Robert Kirkpatrick, et al. 2006. “Sequencing and Analysis of 10,967 Full-Length cDNA Clones from Xenopus Laevis and Xenopus Tropicalis Reveals Post-Tetraploidization Transcriptome Remodeling.” *Genome Research* 16 (6): 796–803.
Najas, Sònia, Juan Arranz, Pamela A. Lochhead, Anne L. Ashford, David Oxley, Jean M. Delabar, Simon J. Cook, María José Barallobre, and Maria L. Arbonés. 2015. “DYRK1A-Mediated Cyclin D1 Degradation in Neural Stem Cells Contributes to the Neurogenic Cortical Defects in Down Syndrome.” *EBioMedicine* 2 (2): 120–34.
Neumann, Fernanda, Stéphanie Gourdain, Christelle Albac, Alain D. Dekker, Linh Chi Bui, Julien Dairou, Isabelle Schmitz-Afonso, et al. 2018. “DYRK1A Inhibition and Cognitive Rescue in a Down Syndrome Mouse Model Are Induced by New Fluoro-DANDY Derivatives.” *Scientific Reports*. https://doi.org/10.1038/s41598-018-20984-z.
Nieuwkoop, P. D., and J. Faber. 1958. “Normal Table of Xenopus Laevis (Daudin).” *Copeia*. https://doi.org/10.2307/1439568.
Ori-McKenney, Kassandra M., Richard J. McKenney, Hector H. Huang, Tun Li, Shan Meltzer, Lily Yeh Jan, Ronald D. Vale, Arun P. Wiita, and Yuh Nung Jan. 2016. “Phosphorylation of β-Tubulin by the Down Syndrome Kinase, Minibrain/DYRK1a, Regulates Microtubule Dynamics and Dendrite Morphogenesis.” *Neuron* 90 (3): 551–63.
Owens, Nick D. L., Ira L. Blitz, Maura A. Lane, Ilya Patrushev, John D. Overton, Michael J. Gilchrist, Ken W. Y. Cho, and Mustafa K. Khokha. 2016. “Measuring Absolute RNA Copy Numbers at High Temporal Resolution Reveals Transcriptome Kinetics in Development.” *Cell Reports* 14 (3): 632–47.
Park, Tae Joo, Brian J. Mitchell, Philip B. Abitua, Chris Kintner, and John B. Wallingford. 2008. “Dishevelled Controls Apical Docking and Planar Polarization of Basal Bodies in Ciliated Epithelial Cells.” *Nature Genetics* 40 (7): 871–79.
Satterstrom, F. Kyle, Jack A. Kosmicki, Jiebiao Wang, Michael S. Breen, Silvia De Rubeis, Joon-Yong An, Minshi Peng, et al. 2020. “Large-Scale Exome Sequencing Study Implicates Both Developmental and Functional Changes in the Neurobiology of Autism.” *Cell*, January. https://doi.org/10.1016/j.cell.2019.12.036.
Shaikh, Mirja N., Francisco Gutierrez-Aviño, Jordi Colonques, Julian Ceron, Barbara Hämmerle, and Francisco J. Tejedor. 2016. “Minibrain Drives the Dacapo-Dependent Cell Cycle Exit of Neurons in the Drosophila Brain by Promoting Asense and Prospero Expression.” *Development* 143 (17): 3195–3205.

Shi, Jianhua, Tianyi Zhang, Chunlei Zhou, Muhammad Omar Chohan, Xiaosong Gu, Jerzy Wegiel, Jianhua Zhou, et al. 2008. “Increased Dosage of Dyrk1A Alters Alternative Splicing Factor (ASF)-Regulated Alternative Splicing of Tau in Down Syndrome.” *The Journal of Biological Chemistry* 283 (42): 28660–69.
Sive, Hazel L., Robert M. Grainger, and Richard M. Harland. 2000. *Early Development of Xenopus Laevis: A Laboratory Manual*. CSHL Press.
Sive, Hazel L., Robert M. Grainger, and Richard M. Harland. 2007. “Synthesis and Purification of Digoxigenin-Labeled RNA Probes for in Situ Hybridization.” *CSH Protocols* 2007 (August): db.prot4778.
Smith, Ian, and Federico Calegari. 2015. “Cyclin D1 Again Caught in the Act: Dyrk1a Links G1 and Neurogenesis in Down Syndrome.” *EBioMedicine* 2 (2): 96–97.
Soppa, Ulf, Julian Schumacher, Victoria Florencio Ortiz, Tobias Pasqualon, Francisco J. Tejedor, and Walter Becker. 2014. “The Down Syndrome-Related Protein Kinase DYRK1A Phosphorylates p27(Kip1) and Cyclin D1 and Induces Cell Cycle Exit and Neuronal Differentiation.” *Cell Cycle* 13 (13): 2084–2100.
Stotani, Silvia, Fabrizio Giordanetto, and Federico Medda. 2016. “DYRK1A Inhibition as Potential Treatment for Alzheimer’s Disease.” *Future Medicinal Chemistry* 8 (6): 681–96.
Tejedor, F., X. R. Zhu, E. Kaltenbach, A. Ackermann, A. Baumann, I. Canal, M. Heisenberg, K. F. Fischbach, and O. Pongs. 1995. “Minibrain: A New Protein Kinase Family Involved in Postembryonic Neurogenesis in Drosophila.” *Neuron* 14 (2): 287–301.
Tu, Fan, Jakub Sedzinski, Yun Ma, Edward M. Marcotte, and John B. Wallingford. 2018. “Protein Localization Screening in Vivo Reveals Novel Regulators of Multiciliated Cell Development and Function.” *Journal of Cell Science*. https://doi.org/10.1242/jcs.206565.
Walentek, Peter, Ian K. Quigley, Dingyuan I. Sun, Umeet K. Sajjan, Christopher Kintner, and Richard M. Harland. 2016. “Ciliary Transcription Factors and miRNAs Precisely Regulate Cp110 Levels Required for Ciliary Adhesions and Ciliogenesis.” *eLife*. https://doi.org/10.7554/elife.17557.
Willsey, A. Jeremy, Montana T. Morris, Sheng Wang, Helen R. Willsey, Nawei Sun, Nia Teerikorpi, Tierney B. Baum, et al. 2018. “The Psychiatric Cell Map Initiative: A Convergent Systems Biological Approach to Illuminating Key Molecular Pathways in Neuropsychiatric Disorders.” *Cell* 174 (3): 505–20.
Willsey, Helen Rankin, Peter Walentek, Cameron R. T. Exner, Yuxiao Xu, Andrew B. Lane, Richard M. Harland, Rebecca Heald, and Niovi Santama. 2018. “Katanin-like Protein Katnal2 Is Required for Ciliogenesis and Brain Development in Xenopus Embryos.” *Developmental Biology* 442 (2): 276–87.
Zhu, Anqi, Joseph G. Ibrahim, and Michael I. Love. 2019. “Heavy-Tailed Prior Distributions for Sequence Count Data: Removing the Noise and Preserving Large Differences.” *Bioinformatics* 35 (12): 2084–92.

Figures:

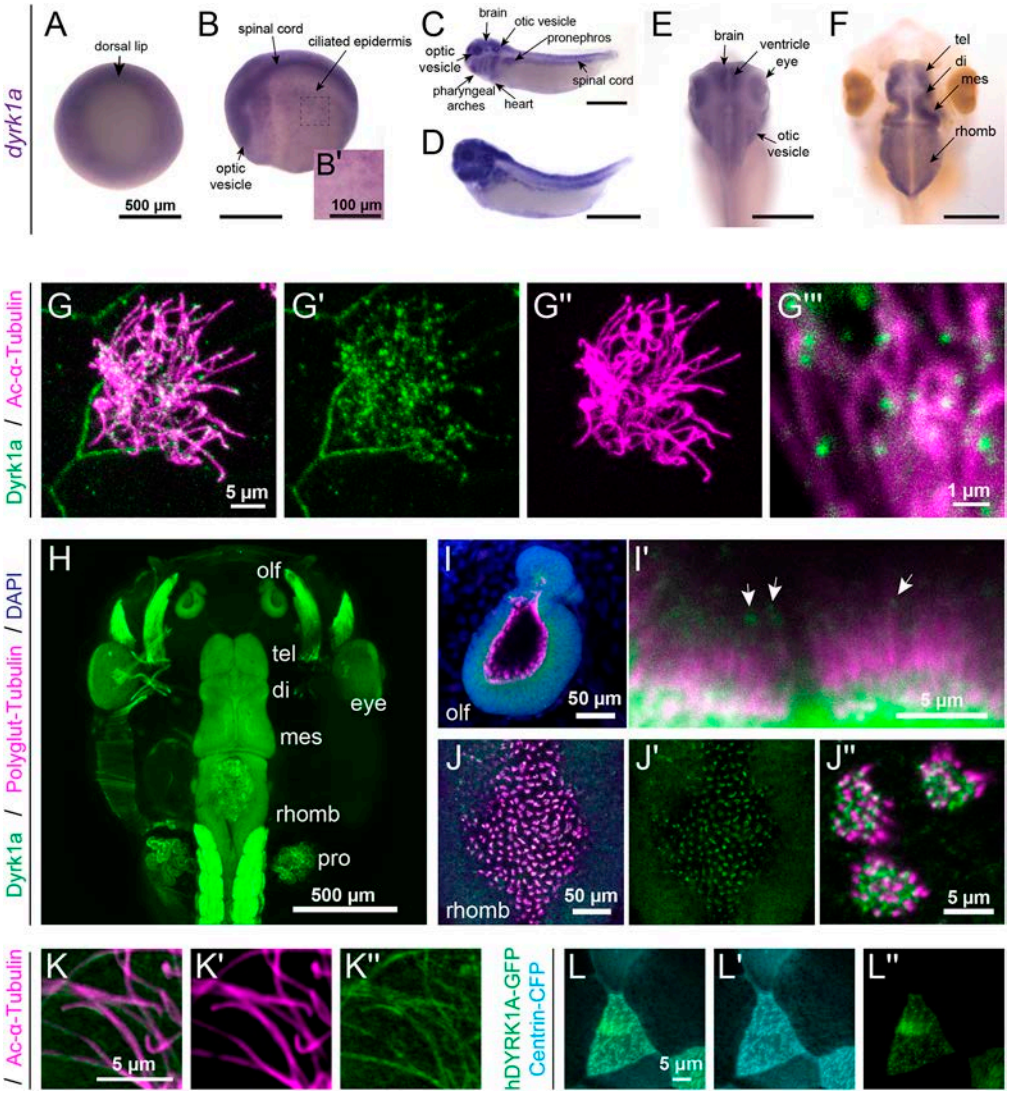

Figure 1: Expression and localization of Dyrk1a during *X. tropicalis* development.

(A-F): By RNA *in situ* hybridization in *X. tropicalis*, *dyrk1a* is expressed during gastrulation (stage 10.5, A) and at stage 20 (B) in the brain, spinal cord, optic vesicles, and ciliated epidermis (B'). At stages 32 (C) and 35 (D), *dyrk1a* is expressed in the brain, spinal cord, otic vesicles, optic vesicles, pharyngeal arches, heart, epidermis, and pronephros. At stages 40 (E) and 46 (F), *dyrk1a* brain expression, especially along ventricles. Telencephalon (tel), diencephalon (di), mesencephalon (mes), and rhombencephalon (rhomb). Scale is 500 µm, except 100 µm in B'. (G) Embryonic epidermis antibody staining for Dyrk1a protein (green) shows puncta along ciliary axonemes labeled by acetylated α-Tubulin (Ac-α-Tubulin, magenta).

See Fig. S1 for antibody validation. (H) Dorsal view of whole-mount antibody staining showing Dyrk1a (green) throughout the nervous system and in the pronephros (pro). (I-J) Dyrk1a (green) is on cilia marked by polyglutamylated-Tubulin (polyglut-Tubulin, magenta) in the olfactory epithelium (olf, I) and in the rhombencephalon (J). White arrows (I') indicate puncta of Dyrk1a (green) on cilia. Also note strong membrane staining. (K) Human GFP-tagged DYRK1A (hDYRK1A-GFP, green) localizes in puncta along ciliary axonemes labeled by acetylated α-Tubulin (magenta). (L) hDYRK1A-GFP (green) co-localizes with Centrin-CFP (cyan) at basal bodies.

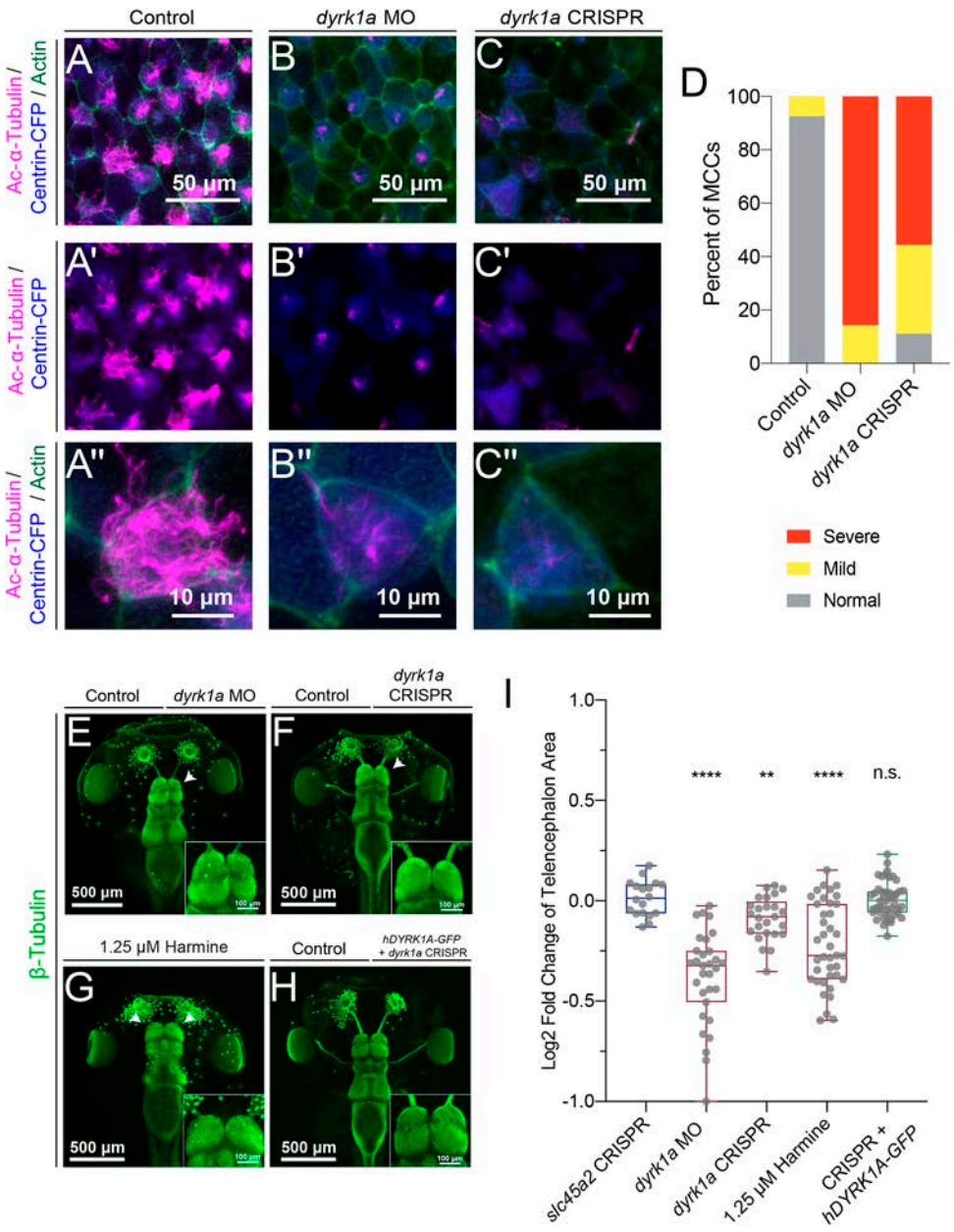

Figure 2: *dyrk1a* is required for ciliogenesis and brain size.

(A-C) Stage 35 *X. tropicalis* embryonic epidermis stained for acetylated α-Tubulin (cilia, magenta), phalloidin (actin, green), and expressing Centrin-CFP (basal bodies, blue). Injection of *dyrk1a* morpholino (MO) (B) or CRISPR/Cas9 reagents (C) causes a loss in cilia (magenta) compared to the injected control (A). See also Fig. S2-S3. (D) Quantification of ciliogenesis phenotype (severe, mild, and normal) in multiciliated cells (MCCs) by condition. n > 35 for each condition. (E-H) Dorsal view of β-Tubulin antibody staining (green) of *X. tropicalis* tadpoles,

injected (right side) with *dyrk1a* morpholino (MO) (E), *dyrk1a* CRISPR (F), or co-injected with *dyrk1a* CRISPR and human GFP-tagged DYRK1A (hDYRK1A-GFP) (H). Dyrk1a kinase inhibitor harmine-treated embryos are affected bilaterally (1.25 µM, G). Telencephalon region shown as insets. White arrows point to telencephalon size phenotypes. (I) Quantification of log2 fold change of telencephalon size normalized to control. Box plot whiskers are maximum and minimums, boxes are interquartile range, and line is median. Every point is an animal. p-values are from non-parametric Mann-Whitney rank sum tests compared to negative control CRISPR targeting pigmentation gene *slc45a2*. For harmine, comparison to paired DMSO treatment also gives a p-value < 0.0001. ** indicates $p < 0.01$; **** indicates $p < 0.0001$; “n.s.” indicates “not significant”, $p > 0.05$.

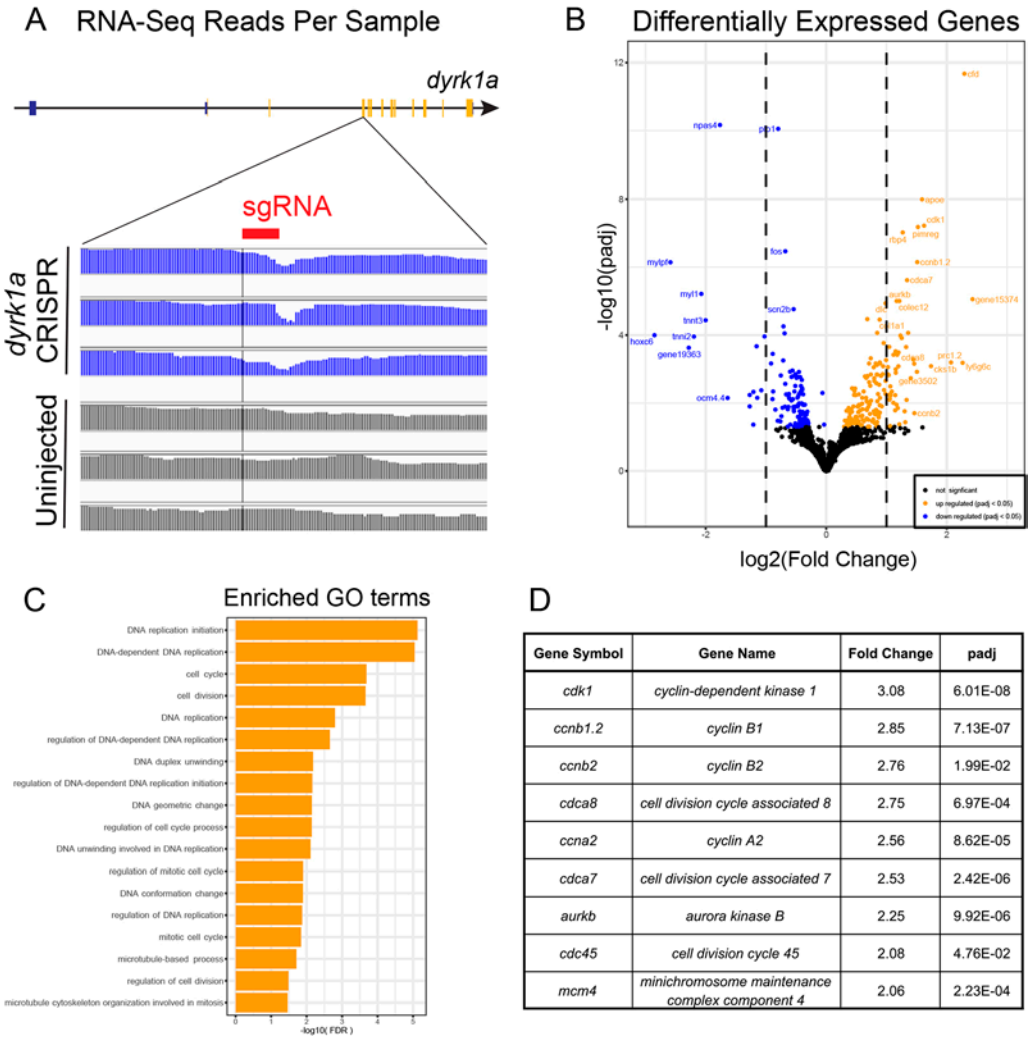

Gene Symbol	Gene Name	Fold Change	padj
cdk1	*cyclin-dependent kinase 1*	3.08	6.01E-08
ccnb1.2	*cyclin B1*	2.85	7.13E-07
ccnb2	*cyclin B2*	2.76	1.99E-02
cdca8	*cell division cycle associated 8*	2.75	6.97E-04
ccna2	*cyclin A2*	2.56	8.62E-05
cdca7	*cell division cycle associated 7*	2.53	2.42E-06
aurkb	*aurora kinase B*	2.25	9.92E-06
cdc45	*cell division cycle 45*	2.08	4.76E-02
mcm4	*minichromosome maintenance complex component 4*	2.06	2.23E-04

Figure 3: RNA sequencing implicates cell cycle control in the *dyrk1a* brain phenotype.
(A) RNA sequencing reads of uninjected control and *dyrk1a* CRISPR samples. These were from dissected stage 46 brains. Note the loss of sequencing reads (blue) adjacent to the sgRNA target site (red) in the injected samples and not the uninjected samples within the targeted exon of *dyrk1a*. (B) Volcano plot of differentially expressed genes (DEGs) following *dyrk1a* mutation with fold change and adjusted p-value in log scales on x- and y-axis. DEGs with p-value < 0.05 are shown for up regulated (orange) and down regulated (blue). (C) Enriched gene ontology (GO) terms of DEGs by false discovery rate (FDR). (D) A list of selected DEGs with high fold change and high significance related to cell cycle control.

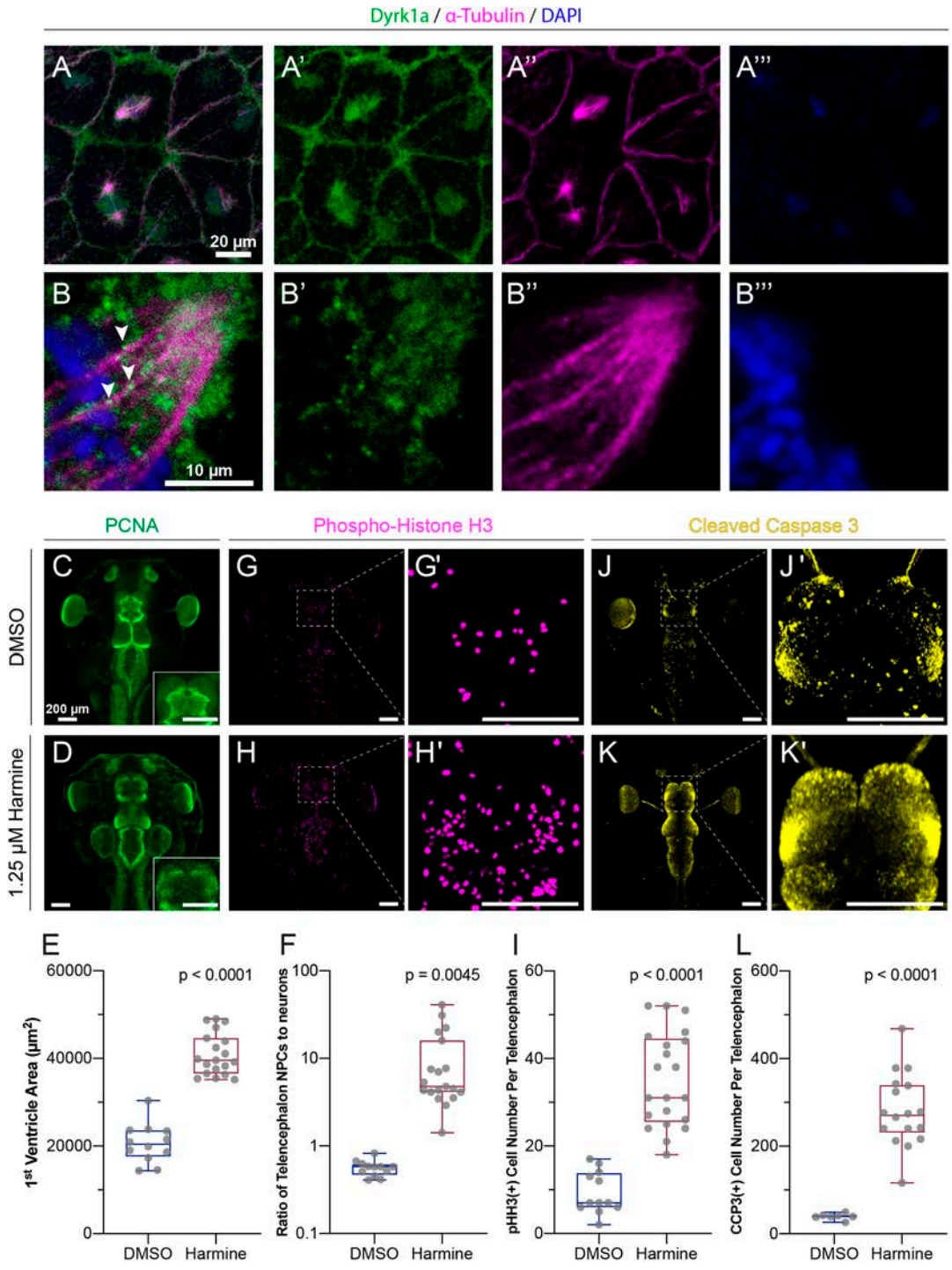

Figure 4: Dyrk1a localizes to mitotic spindles and is required for cell cycle progression and survival. (A-B) Stage 10 embryos stained for Dyrk1a (green), α-Tubulin (microtubules, magenta), and DAPI (DNA, blue). White arrows indicate Dyrk1a puncta near mitotic spindle. (C-L) Dorsal view of *X. tropicalis* tadpoles treated with DMSO (top row) or 1.25 µM Dyrk1a inhibitor

Harmine (bottom row). (C-D) Antibody staining for PCNA (proliferating cell nuclear antigen, S phase marker, green). Telencephalon region shown as an inset. (E) Quantification of first ventricle area from PCNA staining. (F) Quantification of the ratio of neural progenitor cells (NPCs, PCNA area) to the area of differentiated neurons in each telencephalon (log scale). (G-H) Antibody staining for pHH3 (phospho-histone H3, M phase marker, magenta). (G', H') High magnification views of telencephalon regions from G and H. (I) Quantification of pHH3 positive cell number per telencephalon. See also Fig. S4. (J-K) Antibody staining for CCP3 (cleaved caspase 3, cell death marker, yellow). (J', K') High magnification view of telencephalon from J and K. (L) Quantification of CCP3 positive cell number per telencephalon. Scale bars in C-L including insets are 200 µm. Box plot whiskers are maximum and minimum, boxes are interquartile range, and line is median. Every point is an animal. p-values are from non-parametric Mann-Whitney rank sum tests.

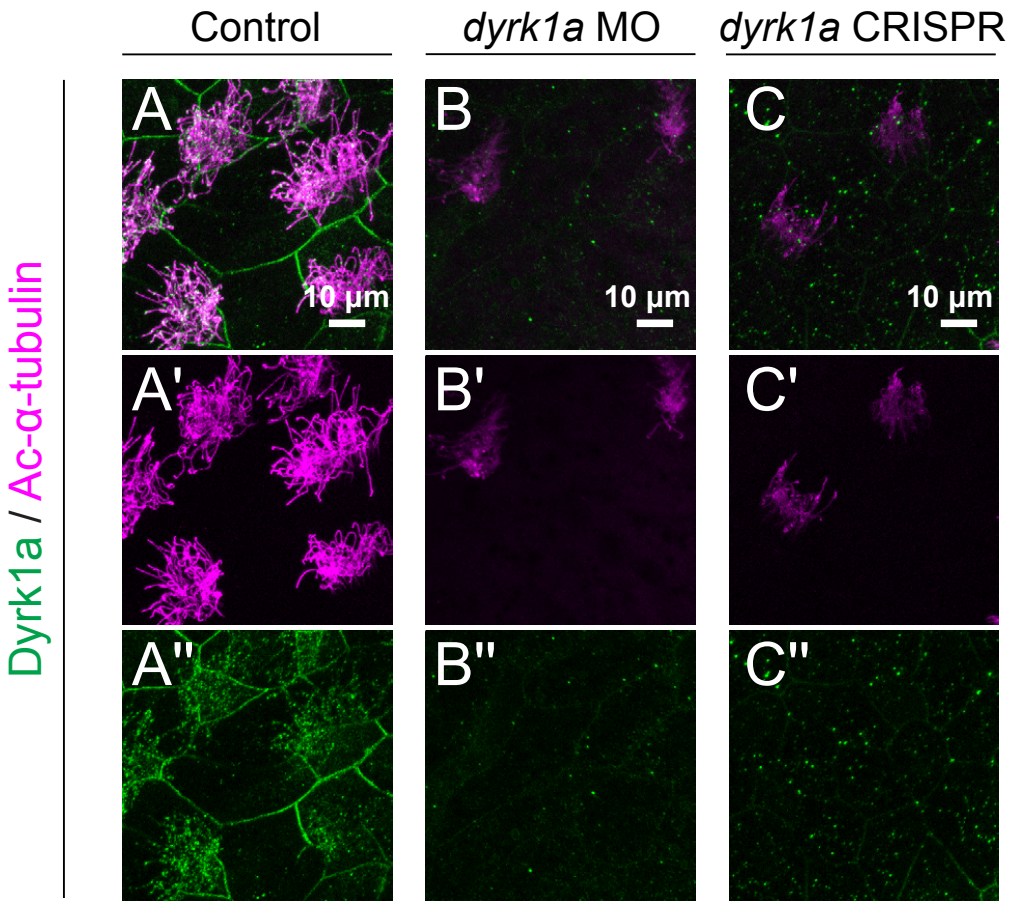

Figure S1: Dyrk1a antibody staining is reduced upon *dyrk1a* perturbation.

(A-C): Acetylated α-Tubulin antibody staining (magenta) and Dyrk1a antibody staining (green) of stage 35 *X. tropicalis* embryonic epidermis. (A) Control injection shows Dyrk1a antibody staining along ciliary axonemes. *dyrk1a* morpholino (MO) (B) or *dyrk1a* CRISPR/Cas9 (C) injection reduces Dyrk1a antibody staining.

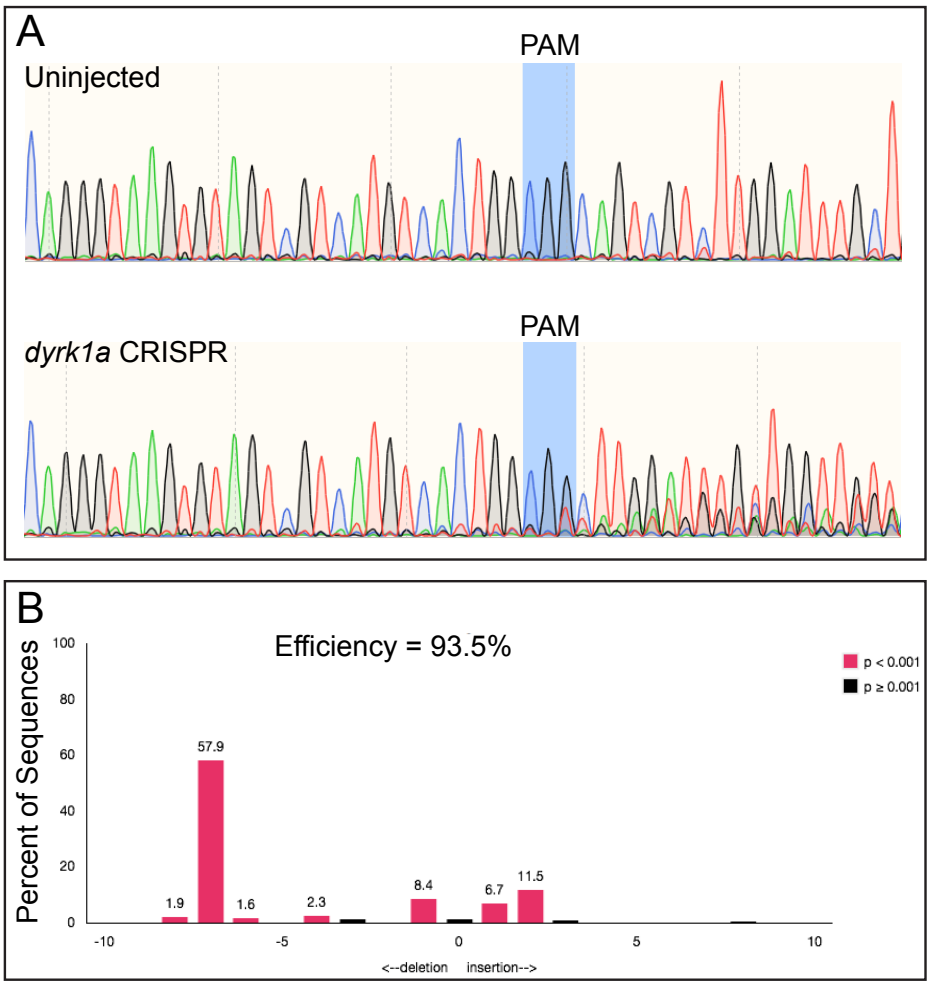

Figure S2: *dyrk1a* CRISPR genotyping.

(A) Examples of Sanger sequencing traces from PCR products amplifying the region surrounding the protospacer adjacent motif (PAM) within the *dyrk1a* coding sequence for uninjected control and *dyrk1a* CRISPR/Cas9 bilaterally injected embryos. Note the drop-off in sequence quality following the PAM, indicating insertions and/or deletions. (B) Example of tracking of INDELs (TIDE) analysis from the injected animal in (A), where Sanger sequencing traces are deconvolved to determine frequency and position of induced variants. For this sample, mutational efficiency is 93.5%, and the frequency and position of insertion and deletion frequency are shown as a histogram. For this sample, the most common sequence was a -7 base pair deletion (57.9% of sequences).

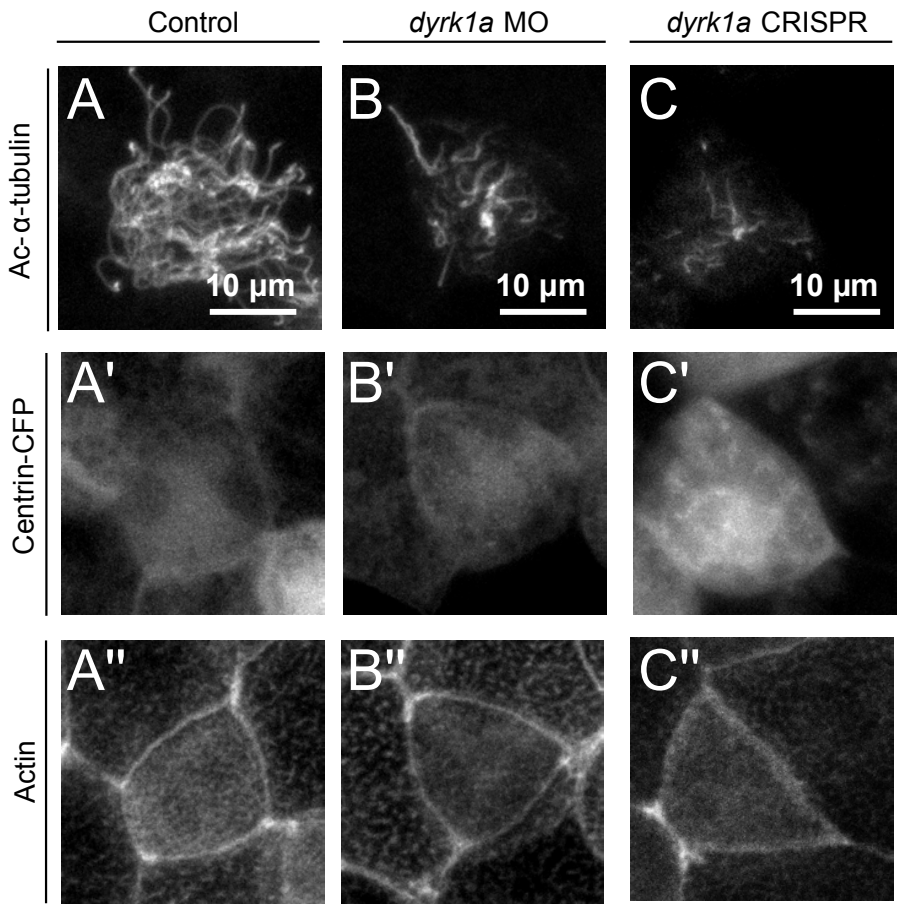

Figure S3: *dyrk1a* is required for ciliogenesis.

(A-C) Separated channels in grayscale from stage 35 *X. tropicalis* embryonic epidermis from Fig. 2. Injection of *dyrk1a* morpholino (MO) (B) or CRISPR/Cas9 reagents (C) causes defects in ciliogenesis compared to the injected control (A).

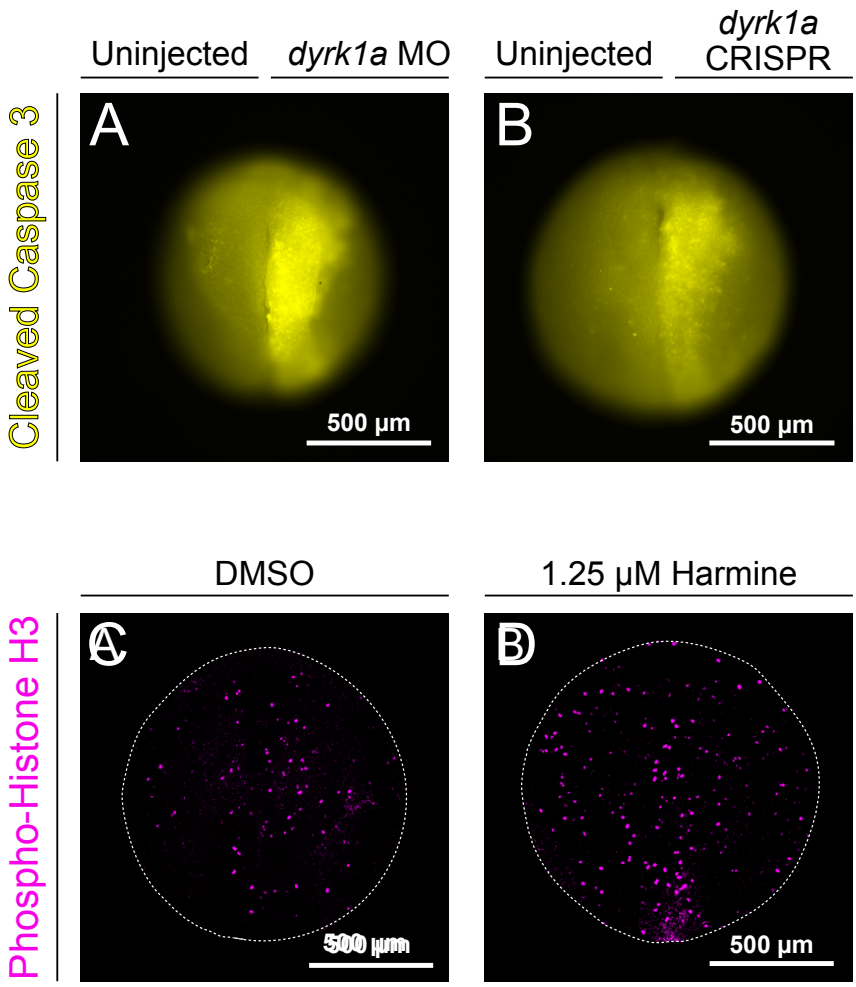

Figure S4: Loss of *dyrk1a* increases cleaved caspase 3 and phospho-histone H3 staining. (A-B) Representative images of cleaved caspase 3 (yellow) staining of *X. tropicalis* neurula stage embryos injected only on the right side with *dyrk1a* morpholino (MO) (A) or *dyrk1a* CRISPR/Cas9 reagents (B). (C-D) Representative images of phospho-histone H3 (magenta) staining of *X. tropicalis* neurula stage embryos treated with DMSO (C) or 10 µM Harmine (D) beginning at blastula stages. Outlines of the embryos are shown in white dashed lines (C-D). All images are dorsal view with the anterior oriented to the top, and maximum intensity projections of optical sections. All conditions have a sample size greater than 20.

Table S1: Differentially expressed genes following *dyrk1a* CRISPR injection.

Xenopus tropicalis gene symbol, log2 fold change, adjusted p-value (padj), and additional information for 294 genes differentially expressed in stage 46 brains following *dyrk1a* CRISPR injection.

Click here to Download Table S1

Table S2: Enriched gene ontology terms from differentially expressed genes following *dyrk1a* CRISPR injection.

Enriched gene ontology terms, fold enrichment, false discovery rate, and differentially expressed (DEX) genes comprising each category for the 221 annotated genes DEX following *dyrk1a* CRISPR injection.

Click here to Download Table S2

Table S3: Differential exon usage following *dyrk1a* CRISPR injection.

Xenopus tropicalis gene symbol, transcript name, exon number, log2 fold change, adjusted p-value (padj), and additional information for the 97 sites of differential exon usage following *dyrk1a* CRISPR injection.

Click here to Download Table S3

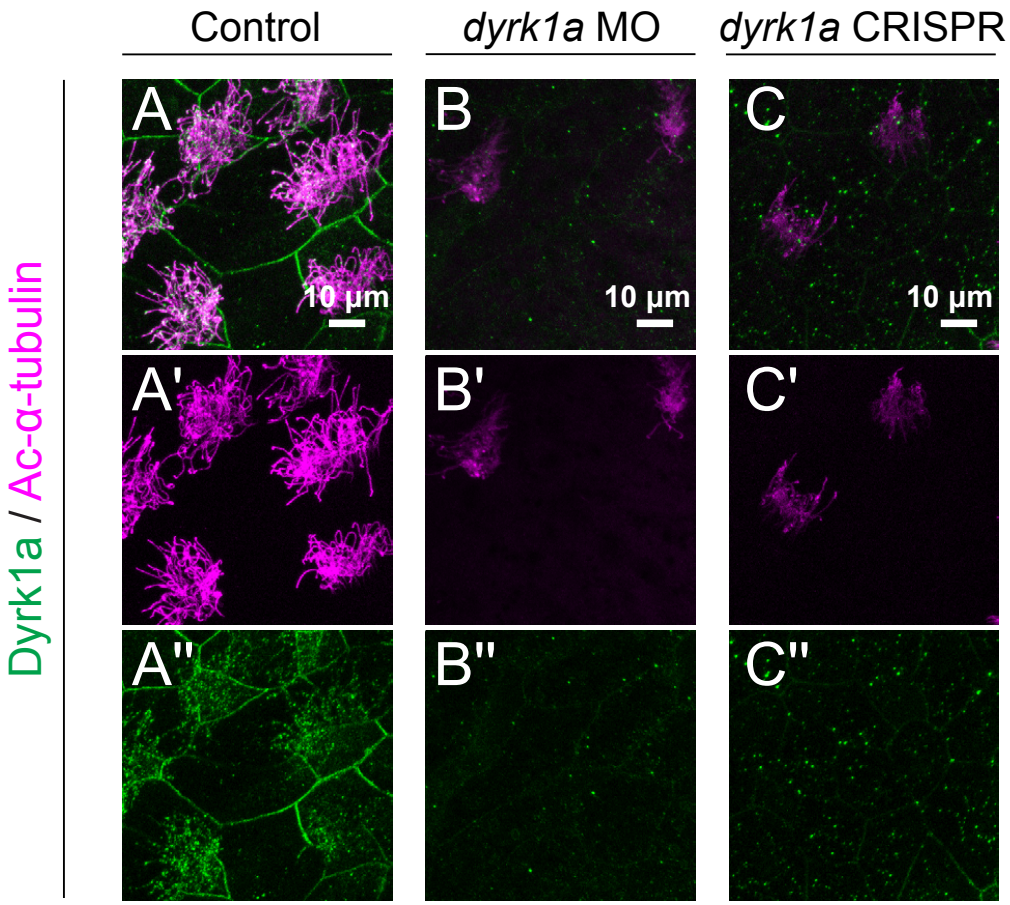

Figure S1: Dyrk1a antibody staining is reduced upon *dyrk1a* perturbation.

(A-C): Acetylated α-Tubulin antibody staining (magenta) and Dyrk1a antibody staining (green) of stage 35 *X. tropicalis* embryonic epidermis. (A) Control injection shows Dyrk1a antibody staining along ciliary axonemes. *dyrk1a* morpholino (MO) (B) or *dyrk1a* CRISPR/Cas9 (C) injection reduces Dyrk1a antibody staining.

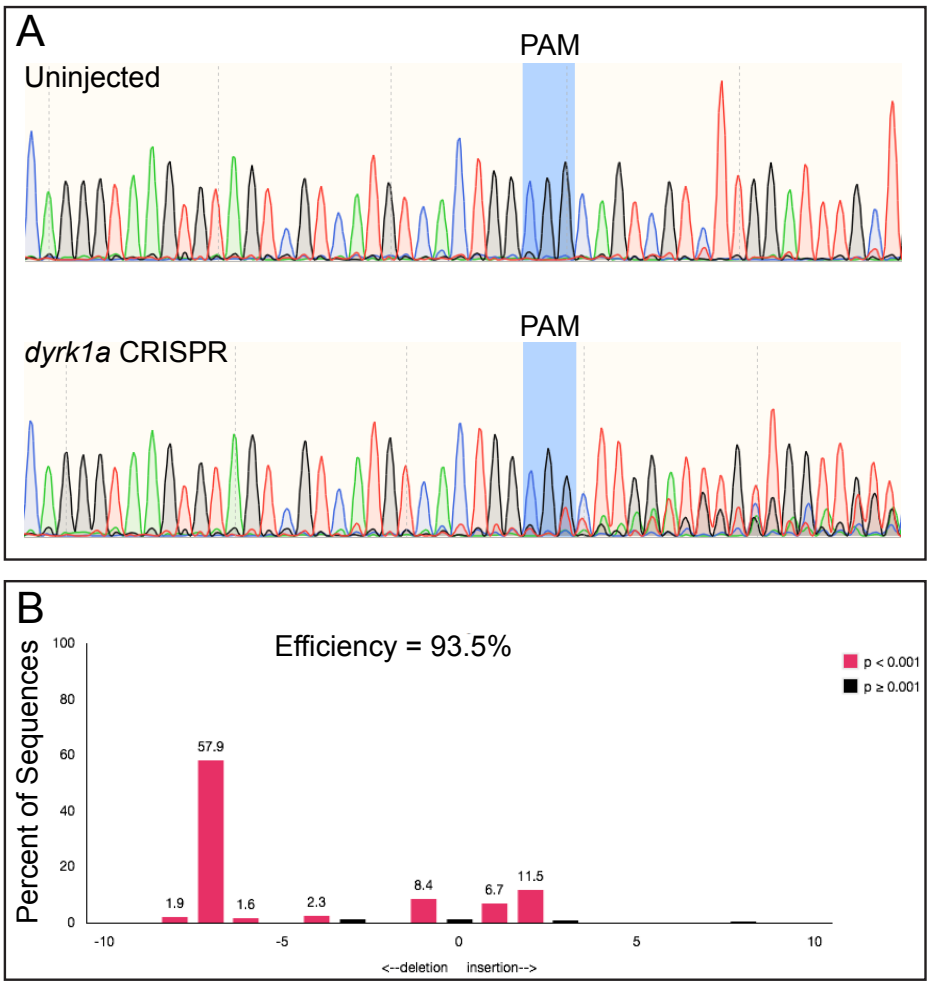

Figure S2: *dyrk1a* CRISPR genotyping.

(A) Examples of Sanger sequencing traces from PCR products amplifying the region surrounding the protospacer adjacent motif (PAM) within the *dyrk1a* coding sequence for uninjected control and *dyrk1a* CRISPR/Cas9 bilaterally injected embryos. Note the drop-off in sequence quality following the PAM, indicating insertions and/or deletions. (B) Example of tracking of INDELs (TIDE) analysis from the injected animal in (A), where Sanger sequencing traces are deconvolved to determine frequency and position of induced variants. For this sample, mutational efficiency is 93.5%, and the frequency and position of insertion and deletion frequency are shown as a histogram. For this sample, the most common sequence was a -7 base pair deletion (57.9% of sequences).

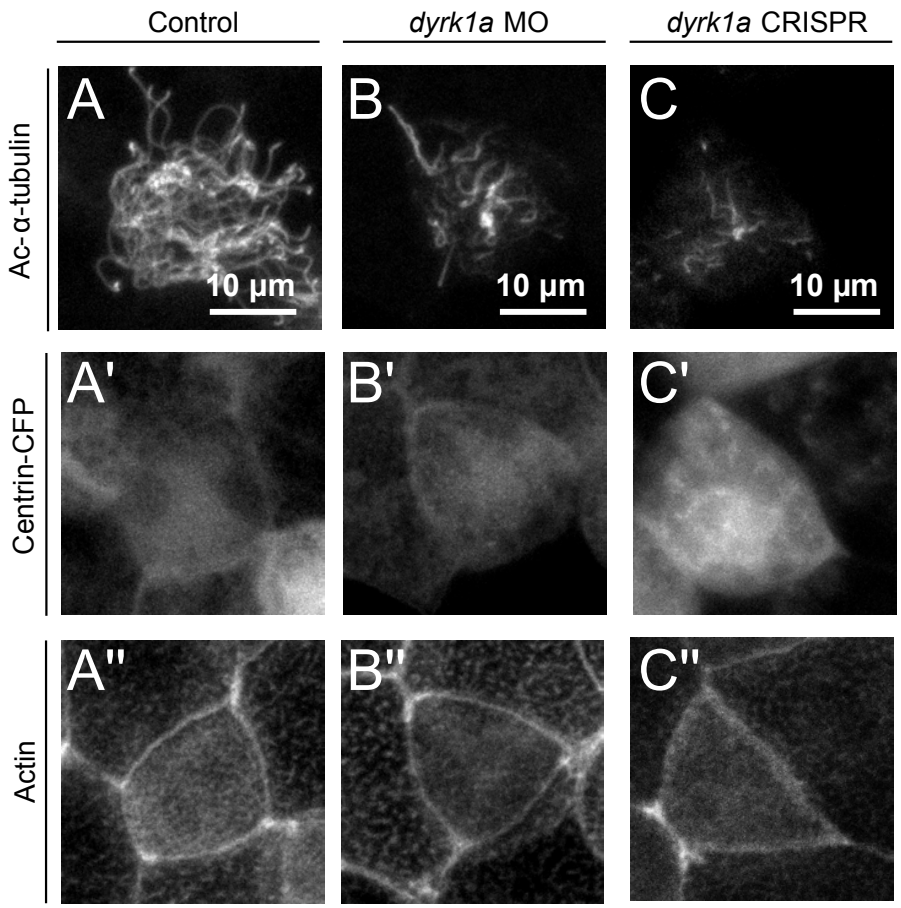

Figure S3: *dyrk1a* is required for ciliogenesis.

(A-C) Separated channels in grayscale from stage 35 *X. tropicalis* embryonic epidermis from Fig. 2. Injection of *dyrk1a* morpholino (MO) (B) or CRISPR/Cas9 reagents (C) causes defects in ciliogenesis compared to the injected control (A).

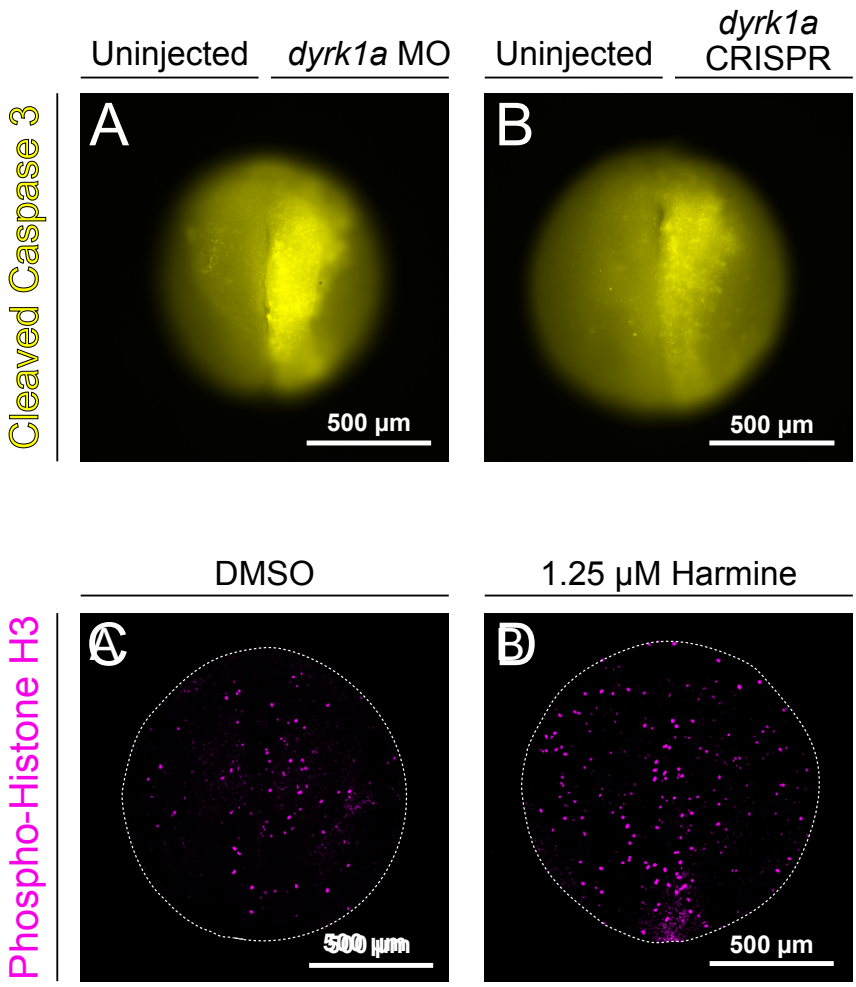

Figure S4: Loss of *dyrk1a* increases cleaved caspase 3 and phospho-histone H3 staining. (A-B) Representative images of cleaved caspase 3 (yellow) staining of *X. tropicalis* neurula stage embryos injected only on the right side with *dyrk1a* morpholino (MO) (A) or *dyrk1a* CRISPR/Cas9 reagents (B). (C-D) Representative images of phospho-histone H3 (magenta) staining of *X. tropicalis* neurula stage embryos treated with DMSO (C) or 10 µM Harmine (D) beginning at blastula stages. Outlines of the embryos are shown in white dashed lines (C-D). All images are dorsal view with the anterior oriented to the top, and maximum intensity projections of optical sections. All conditions have a sample size greater than 20.

Table S1: Differentially expressed genes following *dyrk1a* CRISPR injection.

Xenopus tropicalis gene symbol, log2 fold change, adjusted p-value (padj), and additional information for 294 genes differentially expressed in stage 46 brains following *dyrk1a* CRISPR injection.

Click here to Download Table S1

Table S2: Enriched gene ontology terms from differentially expressed genes following *dyrk1a* CRISPR injection.

Enriched gene ontology terms, fold enrichment, false discovery rate, and differentially expressed (DEX) genes comprising each category for the 221 annotated genes DEX following *dyrk1a* CRISPR injection.

Click here to Download Table S2

Table S3: Differential exon usage following *dyrk1a* CRISPR injection.

Xenopus tropicalis gene symbol, transcript name, exon number, log2 fold change, adjusted p-value (padj), and additional information for the 97 sites of differential exon usage following *dyrk1a* CRISPR injection.

Click here to Download Table S3